

# Receptor noise limitations on chemotactic sensing

Wouter-Jan Rappel<sup>1</sup> and Herbert Levine

Department of Physics and Center for Theoretical Biological Physics, University of California at San Diego, 9500 Gilman Drive, La Jolla, CA 92093

Edited by José N. Onuchic, University of California at San Diego, La Jolla, CA, and approved September 23, 2008 (received for review May 14, 2008)

**Chemotactic eukaryotic cells are able to detect chemoattractant gradients that are both shallow and have a low background concentration. Under these conditions, the noise in the number of bound receptors can be significant and needs to be taken into account in determining the directional sensing process. Here, we quantify numerically the number of bound receptors on the membrane of a disk-shaped cell by using a numerical Monte Carlo tool. The obtained time traces of the receptor occupancy can be used as inputs for any directional sensing model. We investigate the response of the local excitation global inhibition model and a recently developed balanced inactivation model. We determine a measure for the motility of the cell for each model, based on the relevant output variable, as a function of experimental parameters, resulting in several experimentally testable predictions. Furthermore, we show that these two models behave in a qualitatively different fashion when the background concentration is varied. Thus, to properly characterize the sensitivity of cells to receptor occupancy, it is not sufficient to examine the input signal. Rather, one needs to take into account the response of the second messenger pathway.**

chemotaxis | motility

**D**uring eukaryotic chemotaxis, chemical gradients determine and guide the crawling motion of cells. Chemotaxis plays a fundamental role in development and in immune responses and is implicated in the spreading of cancer (1–3). The external gradient of the chemoattractant results in an asymmetric distribution of bound receptors on the cell's membrane and the directional sensing process translates this receptor asymmetry into directed cell motion. A number of biochemical components of the directional sensing pathway of several model systems have been determined (4–7) and an array of different mechanisms have been proposed, including Turing-type instability mechanisms (8), phase separation mechanisms (9), bistable mechanisms (10), depletion mechanisms (11, 12), and communication through diffusible inhibitors (13–16). Despite the recent experimental progress and theoretical efforts, however, the precise mechanisms underlying chemotaxis, in general, and directional sensing, in particular, are poorly understood (17, 18).

Further complicating the directional sensing problem is the potential role of stochasticity. It has been shown that cells are able to chemotax in very shallow gradients with a large range of background concentrations (19, 20). For these shallow gradients the difference in the number of bound receptors at the front and the back of the cell can be as little as 20. Comparing this with the total number of bound receptors, which is of the order of several hundred, leads to the question of noise in directional sensing.

Several recent studies have investigated this issue, by using different approaches, including information theoretical ones (21), general considerations (20, 22, 23) and 1D caricatures of the cell (24). What has been lacking to date, however, is a treatment of the directional sensing problem that (i) exactly quantifies the fluctuations in the number of bound receptors taking into account the spatial extent of the cell and (ii) couples this noisy signal to a downstream intracellular directional sensing pathway.

In this article, we present a numerical modeling study that is able to determine exactly the number of bound receptors as a function of time. These time traces are then used as input signals for a directional sensing pathway. To show the generality of

this approach we investigate here the response of two recently developed intracellular directional sensing models (13, 16). This response is quantified as a function of different experimental parameters, including the background concentration and the ligand diffusion constant, leading to experimentally testable predictions.

## Results

**Time Series.** The first step in our computational procedure is to explicitly generate time series of the number of bound receptors arising from the simple ligand–receptor interaction  $L + R_0 \rightleftharpoons R_1$ . The forward rate  $k_+[L]$ , where  $[L]$  represents the ligand concentration, and backward rate  $k_-$  determine the transitions between the unoccupied  $R_0$  and occupied  $R_1$  states and can be combined to give the dissociation constant  $K_d \equiv \frac{k_-}{k_+}$ . We will consider a cylindrical cell of radius  $R$  where the curved parts are uniformly covered with  $N_{\text{tot}}$  receptors. Motivated by experimental setups, we place this cell in two types of gradients, each with a midpoint, or background concentration of  $c_0$ . The first one, which we will call a linear gradient, is such that the concentration at the front and back differ from the background concentration by a constant amount:  $c_f = c_0 + \Delta$  and  $c_b = c_0 - \Delta$ . The second type is one where the concentration at the front and back is given by  $c_f = c_0(1 + p)$  and  $c_b = c_0(1 - p)$ , respectively. Because this gradient can be approximated by imposing an exponential concentration profile (25) we will call it exponential here.

The cylindrical cell is divided into  $M = 100$  equal-sized radial segments and a typical time series of the number of bound receptors for two of the segments is shown in Fig. 1A for the case of zero gradient. We have verified that the average number of bound receptors is given by the equilibrium value  $N_{\text{seg}}c/(c + K_d)$ , where  $N_{\text{seg}} = N_{\text{tot}}/100$  is the number of receptors of the segment and where  $c$  is the local concentration. Furthermore, we found, as expected, that the variance in the number of bound receptors is  $N_{\text{seg}}cK_d/(c + K_d)^2$ . Parameter values used in this study are based on *Dictyostelium discoideum* data with  $R = 5 \mu\text{m}$ ,  $N_{\text{tot}} = 70,000$ ,  $K_d = 30 \text{ nM}$  and  $k_- = 1 \text{ s}^{-1}$  (26).

Fig. 1B shows the autocorrelation function  $C(t)$  for the total number of bound receptors that can be fitted well with a simple exponential decay:  $C(t) \sim \exp(-t/\tau_c)$ . As has been derived and explicitly shown earlier for spherical cells, the correlation time consists of two contributions  $\tau_c = \tau_{\text{rec}} + \tau_{\text{diff}}$  (27–29). The first one is from the receptor dynamics and is given by the simple relationship  $\tau_{\text{rec}} = 1/(k_- + k_+K_d)$ . The second contribution comes from the diffusive process and depends linearly on the number of receptors and is inversely proportional to the diffusion constant of the ligand:  $\tau_{\text{diff}} = N_{\text{tot}}/(4\pi D_l R K_d)$ . The autocorrelation function for a single segment is also shown in Fig. 1B. The correlation time obtained through an exponential fitting is smaller than the correlation time of the entire cell. The difference between the two correlation times is a result from the nonzero

Author contributions: W.-J.R. and H.L. designed research, performed research, analyzed data, and wrote the paper.

The authors declare no conflict of interest.

This article is a PNAS Direct Submission.

<sup>1</sup>To whom correspondence should be addressed. E-mail: [rappel@physics.ucsd.edu](mailto:rappel@physics.ucsd.edu).

This article contains supporting information online at [www.pnas.org/cgi/content/full/0804702105/DCSupplemental](http://www.pnas.org/cgi/content/full/0804702105/DCSupplemental).

© 2008 by the National Academy of Sciences of the USA

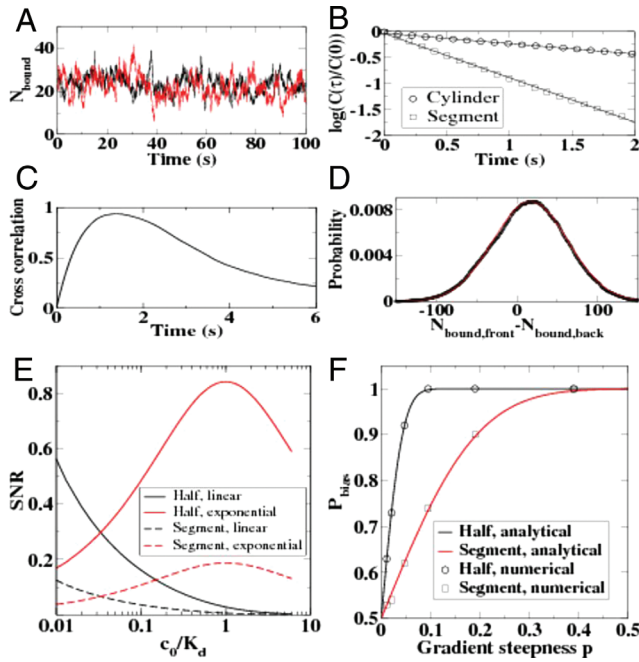


**Fig. 1.** The results from the MCell calculation for  $c_0 = 1$  nM and  $p = 0$  (A–C) and  $p = 0.01$  (D and E). (A) The number of bound receptors as a function of time for two different segments. (B) The normalized correlation function for a single segment (squares) and for the entire cell (circles). The lines are linear fits giving a correlation time for the segment of  $\tau_{c,seg} = 1.18$  s and for the entire cell of  $\tau_{c,cell} = 5.01$  s. (C) The cross-correlation function between neighboring segments, averaged over all pairs, as a function of time. (D) The distribution in the difference between bound receptors in the front and back half of the cell. The symbols are the numerical results and the curve is the Gaussian fit. (E) The signal-to-noise ratio (SNR) for the half and segment comparison as a function of the background concentration for both the linear and exponential gradient. (F) The fraction of the Gaussian distribution which is positive as a function of the exponential gradient steepness. The symbols correspond to values obtained from the MCell simulation and the curves are the results of analytical calculations (see *SI Appendix*). The black curve corresponds to the case where occupancy at the front half and back half of the cell are compared and the red curve corresponds to a comparison between the front-most and back-most segments.

cross-correlation between segments. This cross-correlation is plotted in 1C for neighboring segments and shows a clear maximum at  $t \sim 1.4$  s.

We computed the resulting distribution of the difference in bound receptors between the front half and back half of the cell,  $N_{bound,front} - N_{bound,back}$ , and fitted it to a Gaussian distribution. This is shown in Fig. 1D for the case  $p = 0.02$  where the symbols are obtained from the MCell simulation and the red curve is the Gaussian fit. The fit is excellent and, clearly, the difference is Gaussian distributed. The distribution for each individual segment and, thus, the distribution of the difference between the front-most and back-most segment is also a Gaussian distribution (data not shown). Analytical expression for these distributions can be derived, as shown in the supporting information (*SI Appendix*).

Using the Gaussian distribution, we can quantify the asymmetry in the input signal by calculating the signal-to-noise ratio (SNR), defined as the ratio of the average of the distribution and the standard deviation. Analytical expressions for the SNR can be obtained for both the segment and the halves comparison (see *SI Appendix*). In Fig. 1E we plot the SNR by using these analytical expressions as a function of the background concentration  $c_0$  for a fixed gradient steepness. For a linear gradient (dashed curves), both the halves and the segments decay monotonically as a function of  $c_0$ . For an exponential gradient, however, there is

a maximum at  $c_0 = K_d$ . The SNR for the halves is always larger than the SNR for the segments, reflecting the fact that taking into account more segments improves the ability to separate the front and back signals.

Finally, we have calculated  $P_{bias}$ , defined as the probability that the distribution is  $> 0$  (see *SI Appendix*). This is plotted in Fig. 1F as a function of the exponential gradient steepness  $p$  for both the halves and for the segment comparison. Not surprisingly,  $P_{bias}$  increases as the gradient becomes steeper and is again larger for the halves than for the segments. A comparison between the analytical results (curves) and the numerical results (symbols) demonstrate that the simulation results can be accurately captured by Gaussian distributions.

**Directional Sensing Models.** The output of the stochastic MCell calculations was used as input for two different directional sensing pathway models, the local excitation global inhibition (LEGI) model (13, 14), and the balanced inactivation (BI) model (16). In the LEGI model, the external stimulus produces a local activator as well as a globally diffusing inhibitor. It exhibits perfect adaptation, which ensures that a gradient can be “sensed” for arbitrary background concentration. In the BI model, two second messengers are produced at equal rates. The diffusion of one of them, coupled with an inactivation scheme, ensures a nearly complete suppression of the response at the back and a switch-like response. Because the identification of the biochemical components in the directional sensing mechanisms is problematic, it is impossible to estimate the level of stochasticity arising from fluctuations in the number of second messenger molecules. Hence, the response of these models was simulated by using a deterministic approach in which the cell was taken to be a circle and divided into 100 equal-sized segments. The input on each segment corresponds directly to the number of bound receptors on one of the segments in the MCell simulation.

As a first example of our numerical results we show in Fig. 2A the response of the BI model in the absence of surface diffusion. Here, we plotted the read-out component  $A$  along the perimeter as a function of time in a gray scale, with black corresponding to low values and white corresponding to large values of  $A$ . The response is very jagged, with large values of the response variable (white peaks) on the scale of single-cell segments indicating that a “smoothing” mechanism is needed. The inclusion of nonzero membrane diffusion constant for the read-out component can provide such a mechanism. This is demonstrated in Fig. 2B where the membrane response is smoothed out such that the peak now extends over several segments.

Further examples of our results are found in Fig. 2C–H where we have plotted the response of the two models along the membrane (the variable  $R$  for the LEGI model and  $A$  for the BI model) every second for 100 s for three different values of the exponential gradient  $p$ . Both models experience a much larger and clearer peak in the direction of the gradient for steeper gradients. This is an expected result because the difference in the number of bound receptors increases as the gradient becomes steeper.

To further interpret the results of our simulations we need to construct a motility model. The precise mechanisms by which cells move is complex and poorly understood and involves the actin machinery. Thus, we have chosen to couple our sensing output to a phenomenological model that uses the output at every segment and assigns a velocity to that segment based on the value of the read-out component. Specifically, for the BI model we calculate for each segment  $i$  the following quantity

$$G_i(t) = \frac{1}{T_{dec}} \int_{t-T_{dec}}^t e^{-(t-s)/T_{int}} A_i ds \quad [1]$$

after each “decision” interval  $T_{dec}$ . We have introduced an integration time  $T_{int}$ , which reflects that recent signals contribute more

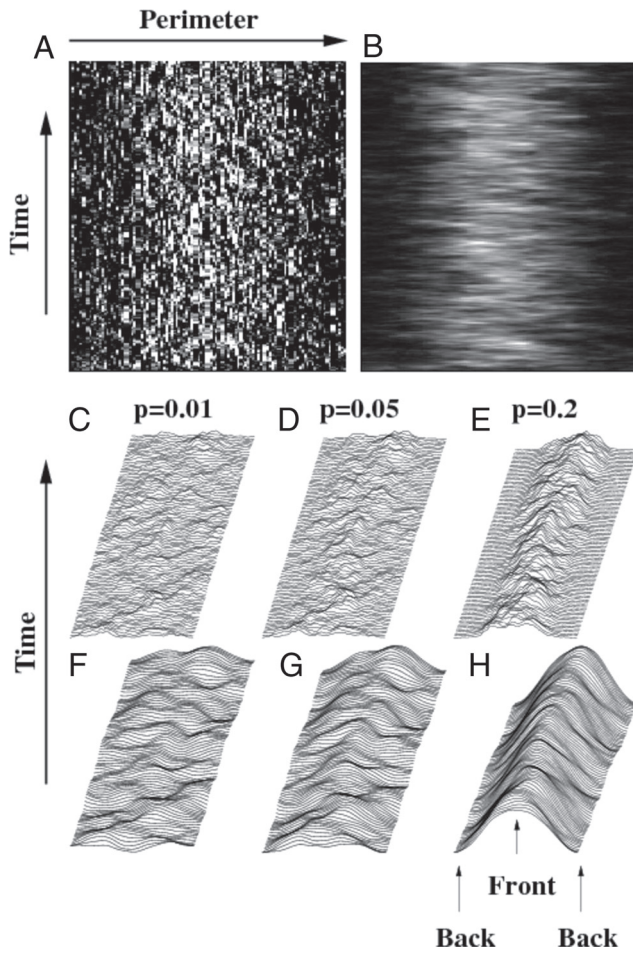


**Fig. 2.** The response of the membrane-bound reporters of the directional sensing models. (A and B) The response of the membrane-bound variable  $A$  of the balanced inactivation model plotted by using a gray scale, with black corresponding to low values of  $A$  and white corresponding to large values of  $A$  ( $p = 0.05$  and  $c_0 = 1$  nM). In A, the membrane diffusion constant of  $A$  was set to be zero and in B it was chosen as  $D_m = 2 \mu\text{m}^2/\text{s}$ . Parameter values for the BI model throughout this study are  $k_a = 10 \text{ s}^{-1}$ ,  $k_i = 1,000 \mu\text{m} (\text{s molecule})^{-1}$ ,  $k_b = 3 \mu\text{m s}^{-1}$ ,  $k_{-a} = 0.2 \text{ s}^{-1}$ ,  $k_{-b} = 0.2 \text{ s}^{-1}$ , and  $D = 10 \mu\text{m}^2\text{s}^{-1}$ . (C–E) The response of  $A$  in the balanced inactivation (C–E) and of the membrane-bound variable  $R$  in the local excitation global inhibition (F–H) model for three different values of the exponential gradient  $p$ . To aid in the visualization, the response was multiplied by a constant factor and shifted in the horizontal and vertical direction. The parameter values for the LEGI model are  $k_{-r} = 10 \mu\text{m} (\text{s molecule})^{-1}$ ,  $k_r = 0.25 \text{ s}^{-1}$ ,  $k_e = 0.1 \text{ s}^{-1}$ ,  $k_{-e} = 0.5 \text{ s}^{-1}$ ,  $k_{-i} = 0.4 \mu\text{m s}^{-1}$ ,  $k_i = 0.4 \text{ s}^{-1}$ ,  $D = 10 \mu\text{m}^2\text{s}^{-1}$  and  $D_m = 1 \mu\text{m}^2\text{s}^{-1}$ .

strongly to motility than signals that occurred in the distant past. From this, we calculate a response function for each decision interval,  $X_i$ , relative to the average value of  $G_i$  over all  $M$  segments:

$$X_i = G_i - \frac{1}{M} \sum_{i=1}^M G_i \quad [2]$$

The contribution of this segment to the overall velocity of the cell is calculated as

$$\begin{aligned} \mathbf{v}_i &= 0 \text{ if } X_i < \phi \\ \mathbf{v}_i &= v_0 \hat{\mathbf{n}} \text{ if } X_i > \phi \end{aligned} \quad [3]$$

where  $\hat{\mathbf{n}}$  is the normal direction of segment,  $v_0$  is the speed (chosen here to be 1) and where  $\phi$  is a threshold. The cell's velocity  $\mathbf{v}$  is determined by the sum of the velocity of all the segments:

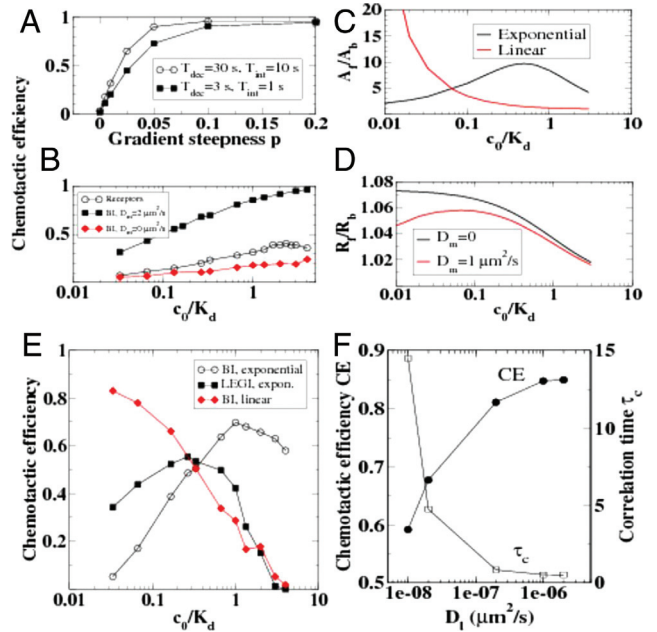


**Fig. 3.** The response of the directional sensing models as a function of system parameters. (A) The chemotactic efficiency as a function of the exponential gradient steepness  $p$  for the BI model for  $c_0 = 1$  nM and motility threshold  $\phi = 0$ . The CE is computed for a short decision interval ( $T_{\text{dec}} = 3$  s, filled squares) and a longer decision interval corresponding to typical pseudopodal lifetimes ( $T_{\text{dec}} = 30$  s, open circles; used in the remainder of the figures). (B) The chemotactic efficiency as a function of the background concentration for the BI model without membrane diffusion (filled diamonds) and with membrane diffusion (filled squares,  $D_m = 2 \mu\text{m}^2/\text{s}$ ) and for the case where the output signal is simply the number of bound receptors in each segment (open circles). The exponential gradient steepness was fixed at  $p = 0.01$  and the threshold value for the motility model was chosen to be  $\phi = 0$ . (C) The ratio of the membrane-bound activator  $A$  in the *deterministic* BI model as a function of  $c_0$  for an exponential gradient ( $p = 0.01$ ) and a linear gradient ( $\Delta = 0.1$  nM). (D) The ratio of the membrane-bound read-out component  $R$  in the *deterministic* LEGI model as a function of  $c_0$  for an exponential gradient with steepness  $p = 0.01$ . The inclusion of a nonzero membrane diffusion constant for the membrane-bound components leads to a maximum in the response curve for small values of  $c_0$  (see also *SI Appendix*). (E) The chemotactic efficiency as a function of the background concentration for the BI model ( $\phi = 0.003$ ) and the LEGI model ( $\phi = 6 \times 10^{-6}$ ). The gradient steepness for the exponential case was fixed at  $p = 0.01$  and for the linear case at  $\Delta = 0.1$  nM. (F) The chemotactic efficiency of the BI model (filled symbols) and the correlation time of a single segment (open symbols) as a function of the ligand diffusion constant ( $c_0 = 1$  nM and  $p = 0.05$ ).

$$\mathbf{v} = \frac{\pi}{M} \sum_{i=1}^M \mathbf{v}_i. \quad [4]$$

where the normalization constant is chosen such that the speed can be at most 1. Cell deformations in this simple model are ignored and the velocity acts on the center of mass of the disk. The chemotactic efficiency  $CE$  is defined as the total displacement in the direction of the gradient divided by the total number of decision intervals and can take on values between  $-1$  and  $+1$ . For the LEGI model we follow an identical procedure with  $A_i$  in Eq. 1 replaced by  $R_i$ . Finally, we have also computed this chemotactic efficiency in the absence of any downstream pathway and where the output signal is the number of bound receptors in each segment (i.e., we substitute  $N_i$  for  $A_i$  in Eq. 1).

In Fig. 3A we show the chemotactic efficiency  $CE$  of the BI model as a function of the steepness parameter  $p$  for exponential gradients ( $c_0 = 1$  nM,  $\phi = 0$ ) for a decision time interval close to typical pseudopodal lifetimes ( $T_{\text{dec}} = 30$  s) and for a much shorter decision time interval ( $T_{\text{dec}} = 3$  s). As expected, the  $CE$

is a sigmoidal function approaching 0 for small values of the gradient steepness and reaching a maximum for steep gradients. Fig. 3A also demonstrates that longer decision intervals and integration times increase the *CE*. This can be expected because a larger integration time is more effective in filtering out the noise than a short integration time. Qualitatively similar curves are obtained in the case for a linear gradient and when applied to the LEGI model (data not shown).

We have investigated the dependence of the *CE* on the background concentration  $c_0$ . Results are shown in Fig. 3B where the *CE* computed solely based on the receptor occupancy is plotted as open circles. This *CE* displays a peak for background concentrations  $\approx 2K_d$  and is larger, for all values of  $c_0$ , than the *CE* computed by using the BI model in the absence of surface diffusion (filled diamonds). However, the inclusion of surface diffusion in the membrane-bound components of the BI model leads to a smoothing of the signal and a significant improvement of the *CE* (filled squares). Qualitatively similar curves can be obtained by using the LEGI model (data not shown).

The curves above were obtained for  $\phi = 0$ , meaning that any segment above the average value contributes equally to the overall motility of the cell. It is more realistic, however, to define a nonzero value for the threshold. Only segments with a value that is significantly above the average will be able to contribute to the formation of actin filaments, generate pseudopods, and affect the cell's velocity. The precise value of this threshold is difficult to determine because the coupling between the directional sensing pathways and the actin pathways is unknown. Here, we pick a threshold that is based on the deterministic response (i.e., the response in the absence of receptor fluctuations) of the directional sensing models. This deterministic response is shown in Fig. 3C and *D*, where we plot the ratio of the membrane-bound indicators at the front and back as a function of  $c_0$  for a fixed value of the gradient steepness  $p$ . For the BI model, the response curve is decreasing monotonically for a linear gradient but shows a maximum at  $c_0 \sim K_d/2$  for an exponential gradient. For the LEGI model, the linear gradient also results in a decreasing ratio as a function of  $c_0$ , independent of the value of  $D_m$  (data not shown). The response of the exponential gradient, however, depends on the value of the membrane diffusion constant. For  $D_m = 0$  the ratio decreases monotonically, a result that can also be obtained analytically (see *SI Appendix*). For nonzero values of  $D_m$ , however, the response of the front is decreased and the curve shows a maximum for small values of  $c_0$ . For the value of  $D_m$  shown in Fig. 3D this maximum occurs at  $c_0 \sim K_d/30$ .

As a threshold value for the motility model we choose 10% of the difference between the front and back value at the maximum in each model. For  $p = 0.01$ , the value considered here, this leads to  $\phi = 0.003$  for the BI model and  $\phi = 6 \times 10^{-6}$  for the LEGI model. This extremely small value for the LEGI model is due to the fact that it only reads the external gradient and leaves the necessary amplification step to an unspecified downstream pathway. The response of the 2 directional sensing models exposed to exponential gradients is shown in Fig. 3E. The BI model displays a clear maximum for values of  $c_0 \sim K_d$  (open circles). The *CE* for the LEGI model peaks for a smaller value of the background concentration (filled squares), reflecting the deterministic curve. Furthermore, it is extremely sensitive to the value of the threshold: it only shows a chemotactic efficiency of  $> 0.5$  at the maximum value of the background concentration for  $\phi < 4 \times 10^{-5}$  (compared with  $\phi < 0.03$  for the BI model). This ultra sensitivity to the threshold value can be improved somewhat by including an amplification step in the LEGI, as was done in Levchenko and Iglesias (14). We have verified that this inclusion does not lead to qualitatively different results (see *SI Appendix*) and that the required threshold is still much smaller than for the BI model ( $\phi \sim 6 \times 10^{-4}$ ). In Fig. 3E we have also plotted the response of the BI model to a linear gradient (filled diamonds) which is maximal for small values of  $c_0$ .

Clearly, the relative difference in occupancy for a linear gradient is much larger for small background concentrations and becomes negligible for large values of  $c_0$  (25). Hence, the *CE* is a decreasing function of the background concentration. A qualitatively similar curve was also found for the LEGI model (data not shown).

We have also investigated the dependence of the correlation time and the *CE* on the ligand diffusion constant  $D_l$  for a fixed value of  $c_0$  and  $p$  (Fig. 3F). Consistent with our earlier numerical work (29), the correlation time of a single segment increases as the ligand diffusion constant is decreased. The *CE* decreases as  $D_l$  is decreased, indicating that the directional sensing becomes more difficult if the ligand molecules diffuse slower.

## Discussion

Motivated by the possible role of receptor fluctuations in eukaryotic chemotaxis, we have explicitly simulated the dynamics of the receptor occupancy. The simulations reported here provide an exact treatment of the input signal for the directional sensing process, including its noise strength, and eliminate the need for approximative approaches. As input parameters, the simulation requires the parameters for the receptor dynamics ( $K_d$  and  $k_-$ ), the geometry of the cell, the number of available receptors, and the diffusion constant of the ligands. We applied our method to a 2D disk-shaped cell but it can be easily extended to arbitrarily shaped cells, including 3D cell shapes although this becomes computationally more expensive. The resulting time series from this method can be used as input for any second messenger pathway. Here, we have studied two different directional sensing mechanisms that use the gradient in receptor occupancy and translate this into an internal second-messenger asymmetry.

The downstream pathway in our study was treated deterministically, ignoring any stochasticity arising from cytosolic diffusion and other signaling pathway reactions, for two reasons. First, the level of this noise will depend critically on the concentration of signaling molecules in the downstream directional sensing pathways. The precise biochemical identification of the components of these pathways is still lacking and the copy number of these components is thus still undetermined. Second, there is no obvious reason to expect this noise to be particularly large; unlike the case of genetic systems, there are very small numbers of the relevant nucleic acids. In any case, including only receptor noise gives an upper bound on the chemotactic efficiency.

A number of other studies have also recognized the importance of noise in directional sensing (20–24). Several of these attempt to estimate the SNR of the input signal, taken to be the difference between the number of bound receptors at the front and at the back of the cell (20, 23). This approach makes a number of assumptions and arrives at an estimated SNR that is a function of the correlation time, the measuring time, and the correlation time of the internal pathways. It is similar to using the results in Fig. 1D and E and determining the chemotactic efficiency uniquely on the basis of the input signal. One difference, however, is that this approach only examines the receptor dynamics and does not capture the contribution of the diffusive process of the ligands to the correlation time and to the SNR. This contribution is small for large diffusion constants but can become important if the diffusion constant of the chemoattractant is lowered (see Fig. 3F). In addition, determining the chemotactic efficiency based on the difference of bound receptors in the front and back assumes that the cell can only move forward or backward and neglects any movement away from the gradient axis. To allow the cell to move in directions other than forward or backward we have introduced a motility model that can be used to quantify a chemotactic efficiency based on the occupancy of the segments (see Eq. 1). The results show that the *CE* has now a maximum for larger background concentrations than based on the SNR (Fig. 3B). Most importantly, however, this approach ignores the downstream sensing pathways and assumes that the cell is somehow able to pick its

direction solely based on the distribution of occupied receptors. As we demonstrate in Fig. 3E, details of the directional sensing models lead to qualitatively different curves. Thus, examining only the input signal is not sufficient and the downstream pathway needs to be taken into account.

In a previous study, we applied our methodology to a simplified geometry in which the cell was represented by two points (the front and the back) connected by a line on which the cytosolic inhibitor can diffuse (24). Although this approach is useful in obtaining insight into the mechanisms of noise propagation, it can not capture the importance of a “smoothing” mechanism. Without such a mechanism, the response along the membrane is very jagged with peaks and valleys occurring on the scale of the segments (see Fig. 24). We show here that diffusion of membrane-bound components of the downstream pathway, with diffusion constants that are consistent with typical values for membrane-bound molecules, is a possible smoothing mechanism. Interestingly, including membrane diffusion of the receptors with a comparable diffusion constant ( $1 \mu\text{m}^2/\text{s}$ ) is not sufficient to smooth the response along the membrane (data not shown). We can provide a rough estimate of the required value of the membrane diffusion constant to eliminate peaks on the scale of the membrane segments in our simulations. For the parameter values used in the BI model, the response time  $\tau_{\text{res}}$  of the activator  $A$ , defined as the time it takes to reach its peak after a sudden increase in the signal, is on the order of 1 s. During this time the molecule diffuses over a length  $\sqrt{D_m \tau_{\text{res}}}$ . This length needs to be at least on the order of the size of a segment  $2\pi R/100 \sim 0.3 \mu\text{m}$ , giving us a lower bound on the diffusion constant of approximately  $0.1 \mu\text{m}^2/\text{s}$  for our numerical approximations to be accurate.

Our study leads to several clear experimental predictions and tests. The first one is shown in Fig. 3F, which demonstrates that the chemotactic efficiency is a function of the correlation time. In particular, the chemotactic efficiency decreases as the correlation time increases, consistent with our findings in 1D (24) and theoretical work on the propagation of noise in signal transduction networks (22, 30). This correlation time is the sum of two terms, one that describes the receptor dynamics and the other one that arises from the ligand diffusion. The second term is inversely proportional to the ligand diffusion constant (28, 29) and changing the correlation time in experiments might be achieved via the chemical modification of the chemoattractant. For example, in the case of *Dictyostelium* it might be possible to tether cAMP to large molecules, whereas in the case of neutrophils large molecules could be attached to the chemoattractant fMLP. These modifications should allow one to reduce the diffusion constant significantly.

The second experimental test can be derived from Fig. 3E, which shows that the response to the noisy input can be model dependent. In particular, the chemotactic efficiency in exponential gradients calculated by using the BI model displays a maximum for a background concentration that is larger than for the LEGI model. Using microfluidic devices (19, 25, 31), possibly combined with uncaging techniques (32), it should be feasible to measure the chemotactic response as a function of the background concentration. The results of these experiments can then be used to critically test the proposed mechanisms, a useful result in light of the current abundance of abstract models. Finally, we should stress here that the obtained time series for the occupied receptors can be used as input in any directional sensing model. As such, it should be possible to use our method to test additional proposed mechanisms and to further restrict the number of viable models.

## Methods

**Generation of Time Traces.** To obtain the time series of the number of bound receptors we use MCell3, a modeling tool for realistic simulations of cellular signaling in complex 3D geometries (33). This simulation tool, recently used by us to characterize the noise level as a function of the number of receptors for a spherical cell (29), uses highly optimized Monte Carlo algorithms to track the stochastic behavior of discrete molecules in space and time as they

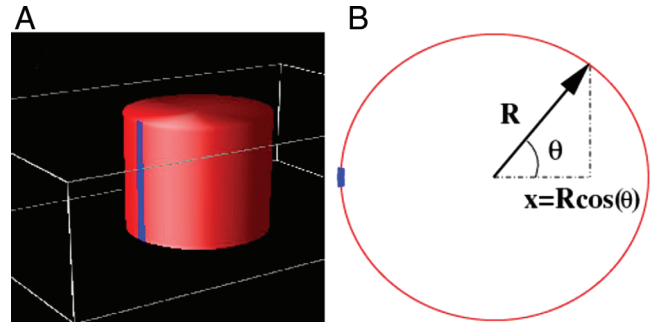


**Fig. 4.** Representation of the numerical procedure. (A) Geometry used in the MCell simulations. A cylindrical cell is placed in a larger computational box of equal height. The cylinder is divided into 100 identical radial segments and the number of receptors is recorded in each segment as a function of time. (B) The time series for each segment is used as input in a 2D simulation of the directional sensing model.

diffuse in user-specified geometries. It can model interactions between diffusing molecules and receptors on cell membranes as well as molecule–molecule interactions and has been validated extensively (33).

Our cylindrical cell is placed in a computational box of equal height and is divided into 100 equally large segments as shown in Fig. 4A. The top, bottom, and sides of the computational box are chosen to be reflective, whereas the front and back are kept at a specified concentration. The ligand molecules diffuse freely in the computational box with a diffusion constant  $D$  that can be set at the start of each simulation, leading to the standard diffusion equations for the ligand concentration:

$$\frac{\partial[L]}{\partial t} = D\nabla^2[L] \quad [5]$$

The MCell simulations record the number of bound receptors  $N_i$  in each segment  $i$  as a function of time. Typical runs lasted 5,000 s for small  $c_0$ , with occupancy recorded every 0.001 s. For larger  $c_0$ , the runs were terminated after 1,000 s. The data were used to calculate the auto correlation function for segment  $i$ ,  $C(\tau) = \int (N_i(t) - \bar{N}_i)(N_i(t + \tau) - \bar{N}_i) dt$ , where  $\bar{N}_i$  is the time-averaged occupancy of the segment. Similarly, the cross-correlation between neighboring segments was calculated as  $C_{\text{cross}}(\tau) = \int (N_i(t) - \bar{N}_i)(N_{i+1}(t + \tau) - \bar{N}_{i+1}) dt$ .

The generation of a gradient in the membrane occupancy was achieved by using two different methods. In the first, our main method, we set the front and back concentration of the computational box equal to  $c_0$ , corresponding to  $p = 0$ , and adjusted the occupancy rate according to the desired gradient. Specifically, we adjust the occupancy for the segment  $\tilde{N}(x, t)$  such that the equilibrium value corresponds to the local concentration value:

$$N(x, t) = \tilde{N}(x, t) \frac{\frac{c(x)}{c(x) + K_d}}{\frac{c_0}{c_0 + K_d}} \quad [6]$$

where  $c(x)$  is the concentration at location  $x$  along the gradient direction with  $x = 0$  corresponding to the cell's center (see Fig. 4B). Thus, for a linear gradient we choose  $c(x) = c_0 + \frac{\Delta c}{R}x$ , whereas for the exponential gradient we have  $c(x) = c_0(1 + \frac{p_{\text{eff}}x}{R})$ .

In the second method, we fixed the concentration at the front and at the back of the computational box corresponding to the desired gradient. The no-flux boundary condition at the cell membrane, however, leads to a distortion of the linear gradient close to the cell (specifically, the derivative of the concentration field normal to the cell's membrane is zero). The actual gradient in the membrane occupancy  $p$  was calculated by fitting the occupancy of the segments to the expression  $N(x) = N_0 + \delta \frac{x}{R}$  where we have used the fact that the position of the segment is given by  $x = R \cos(\theta)$  (see Fig. 4B). Here,  $N_0$  is the equilibrium occupancy in the absence of a gradient and  $\delta$  is a fitting parameter that can be related to the gradient steepness by using the equilibrium values for the occupancy. Specifically, at the front we have  $c_f = c_0(1 + p_{\text{eff}})$  and  $N_f = N_{\text{seg}} c_f / (c_f + K_d)$ . Matching this expression to  $N(R) = N_0 + \delta$  and repeating this procedure for the back we find  $c_b$  and  $c_f$  from which we can determine  $p_{\text{eff}} = (c_f - c_b)/2$ . Importantly, the results from both methods agree well with each other.

**Simulation of the Directional Sensing Models.** The time series obtained by MCell were used as input for a 2D directional sensing simulation where each segment on the cylinder maps onto a segment of the circular cell perimeter (see Fig. 4B). The intracellular pathway is computed by using the phase field method, a method that is particularly well suited to handle the required boundary condition on the curved cell membrane (16, 34, 35).

The first model, the local excitation global inhibition (LEGI) model, assumes that the communication between different parts of the cell is achieved via a diffusible inhibitor whereas the excitation is a local phenomenon (13, 14). Furthermore, perfect adaptation is implemented to ensure that the response can be accomplished over a wide range of gradient parameters. We will use here a simple version of the LEGI model (36), which leaves out any potential downstream amplification steps:

$$\begin{aligned}\frac{\partial E}{\partial t} &= -k_{-e}E + k_eS + D_m \nabla_m^2 E \quad \text{at the membrane} \\ \frac{\partial R}{\partial t} &= -k_{-r}R + k_rE + D_m \nabla_m^2 R \quad \text{at the membrane} \\ \frac{\partial I}{\partial t} &= D \nabla^2 I \quad \text{in the cytosol}\end{aligned}$$

with a boundary condition for the outward-pointing normal derivative of the cytosolic component:

$$D \frac{\partial I}{\partial n} = k_i S - k_{-i} I, \quad [7]$$

where  $S$  is the input signal,  $I$  is the cytosolic inhibitor with diffusion constant  $D$ ,  $E$  is the activator, and  $R$  is the read-out signal. Both  $E$  and  $R$  are membrane bound and can diffuse with a diffusion constant  $D_m$ .

Our second model is the balanced inactivation (BI) model, which also assumes the existence of a diffusible cytosolic inhibitor ( $B$ ) (16). This inhibitor,

produced by the signal  $S$ , suppresses the activation on the membrane, measured by the variable  $A$  through its membrane bound version  $B_m$ .

$$\begin{aligned}\frac{\partial A}{\partial t} &= k_a S - k_{-a} A - k_i A B_m + D_m \nabla_m^2 A \quad \text{at the membrane} \\ \frac{\partial B_m}{\partial t} &= k_b B - k_{-b} B_m - k_i A B_m + D_m \nabla_m^2 B_m \quad \text{at the membrane} \\ \frac{\partial B}{\partial t} &= D \nabla^2 B \quad \text{in the cytosol}\end{aligned}$$

together with

$$D \frac{\partial B}{\partial n} = k_a S - k_b B. \quad [8]$$

Again, the membrane-bound components can diffuse with diffusion constant  $D_m$ . If the diffusion of the cytosolic inhibitor is fast enough the levels of membrane-bound  $B$  at the front and the back are nearly identical. This leads to an almost complete inactivation of  $A$  at the back, whereas the level  $A$  at the front remains significantly nonzero. The resulting large asymmetry in  $A$  can be achieved over a wide range of gradient and model parameters. Further details of this model can be found in the original reference (16).

**ACKNOWLEDGMENTS.** We thank Dr. Tom Bartol for advice on MCell3 and Dr. William F. Loomis for discussions. This work was supported by the National Institutes of Health Grant P01 GM078586.

- Clark R (1996) *The Molecular and Cellular Biology of Wound Repair* (Plenum, New York).
- Dormann D, Weijer CJ (2003) Chemotactic cell movement during development. *Curr Opin Genet Dev* 13:358–364.
- Condeelis JS, Singer RH, Segall JE (2005) The great escape: When cancer cells hijack the genes for chemotaxis and motility. *Annu Rev Cell Dev Biol* 21:695–718.
- Firtel RA, Meili R (2000) Dictyostelium: A model for regulated cell movement during morphogenesis. *Curr Opin Genet Devel* 10:421–427.
- Srinivasan S, et al. (2003) Rac and cdc42 play distinct roles in regulating pi(3,4,5)p3 and polarity during neutrophil chemotaxis. *J Cell Biol* 160:375–385.
- Franca-Koh J, Devreotes PN (2004) Moving forward: Mechanisms of chemoattractant gradient sensing. *Physiology (Bethesda)* 19:300–308.
- Kimmel AR, Firtel RA (2004) Breaking symmetries: Regulation of dictyostelium development through chemoattractant and morphogen signal-response. *Curr Opin Genet Dev* 14:540–549.
- Meinhardt H (1999) Orientation of chemotactic cells and growth cones: Models and mechanisms. *J Cell Sci* 112:2867.
- Gamba A, et al. (2005) Diffusion-limited phase separation in eukaryotic chemotaxis. *Proc Natl Acad Sci USA* 102:16927–16932.
- Mori Y, Jilkine A, Edelstein-Keshet L (2008) Wave-pinning and cell polarity from a bistable reaction-diffusion system. *Biophys J* 94:3684–3697.
- Postma M, van Haastert PJM (2001) A diffusion-translocation model for gradient sensing by chemotactic cells. *Biophys J* 81:1314–1323.
- Narang A, Subramanian KK, Lauffenburger DA (2001) A mathematical model for chemoattractant gradient sensing based on receptor-regulated membrane phospholipid signaling dynamics. *Ann Biomed Eng* 29:677–691.
- Parent CA, Devreotes PN (1999) A cell's sense of direction. *Science* 284:765–770.
- Levchenko A, Iglesias PA (2002) Models of eukaryotic gradient sensing: Application to chemotaxis of amoebae and neutrophils. *Biophys J* 82:50–63.
- Skupsky R, Losert W, Nossal RJ (2005) Distinguishing modes of eukaryotic gradient sensing. *Biophys J* 89:2806–2823.
- Levine H, Kessler DA, Rappel WJ (2006) Directional sensing in eukaryotic chemotaxis: A balanced inactivation model. *Proc Natl Acad Sci USA* 103:9761–9766.
- Chisholm RL, Firtel RA (2004) Insights into morphogenesis from a simple developmental system. *Nat Rev Mol Cell Biol* 5:531–541.
- Iglesias PA, Devreotes PN (2008) Navigating through models of chemotaxis. *Curr Opin Cell Biol* 20:35–40.
- Song L, et al. (2006) *Dictyostelium discoideum* chemotaxis: Threshold for directed motion. *Eur J Cell Biol* 85:981–989.
- van Haastert PJ, Postma M (2007) Biased random walk by stochastic fluctuations of chemoattractant-receptor interactions at the lower limit of detection. *Biophys J* 93:1787–1796.
- Andrews BW, Iglesias PA (2007) An information-theoretic characterization of the optimal gradient sensing response of cells. *PLoS Comput Biol* 3:e153.
- Shibata T, Fujimoto K (2005) Noisy signal amplification in ultrasensitive signal transduction. *Proc Natl Acad Sci USA* 102:331–336.
- Ueda M, Shibata T (2007) Stochastic signal processing and transduction in chemotactic response of eukaryotic cells. *Biophys J* 93:11–20.
- Rappel W-J, Levine H (2008) Receptor noise and directional sensing in eukaryotic chemotaxis. *Phys Rev Lett* 100:228101.
- Herzmark P, et al. (2007) Bound attractant at the leading vs. the trailing edge determines chemotactic prowess. *Proc Natl Acad Sci USA* 104:13349–13354.
- Ueda M, Sako Y, Tanaka T, Devreotes PN, Yanagida T (2001) Single-molecule analysis of chemotactic signaling in *Dictyostelium* cells. *Science* 294:864–867.
- Berg HC, Purcell EM (1977) Physics of chemoreception. *Biophys J* 20:193–219.
- Bialek W, Setayeshgar S (2005) Physical limits to biochemical signaling. *Proc Natl Acad Sci USA* 102:10040–10045.
- Wang K, Rappel WJ, Kerr R, Levine H (2007) Quantifying noise levels of intercellular signals. *Phys Rev E* 75:061905.
- Paulsson J (2004) Summing up the noise in gene networks. *Nature* 427:415–418.
- Jeon NL, et al. (2002) Neutrophil chemotaxis in linear and complex gradients of interleukin-8 formed in a microfabricated device. *Nat Biotechnol* 20:826–830.
- Beta C, Wyatt D, Rappel WJ, Bodenschatz E (2007) Flow photolysis for spatiotemporal stimulation of single cells. *Anal Chem* 79:3940–3944.
- Stiles JR, Bartol TM (2001) Monte Carlo methods for simulating realistic synaptic microphysiology using MCell. *Computational Neurobiology: Realistic Modeling for Experimentalists*, ed de Schutter E (CRC, Boca Raton, FL).
- Kockelkoren J, Levine H, Rappel WJ (2003) Computational approach for modeling intra- and extracellular dynamics. *Phys Rev E* 68:037702.
- Levine H, Rappel WJ (2005) Membrane-bound Turing patterns. *Phys. Rev. E* 72:061912.
- Kutscher B, Devreotes P, Iglesias PA (2004) Local excitation, global inhibition mechanism for gradient sensing: An interactive applet. *Sci STKE* 2004 pl3.